# Towards a parameter-free method for high Reynolds number turbulent flow simulation based on adaptive finite element approximation

Johan Hoffman

*Computational Technology Laboratory*
*Department of High Performance Computing and Visualization*
*School of Computer Science and Communication*
*Stockholm, Sweden*

**Abstract**

We present work towards a parameter-free method for turbulent flow simulation based on adaptive finite element approximation of the Navier-Stokes equations at high Reynolds numbers. In this model, viscous dissipation is assumed to be dominated by turbulent dissipation proportional to the residual of the equations, and skin friction at solid walls is assumed to be negligible compared to inertial effects. The result is a computational model without empirical data, where the only parameter is the local size of the finite element mesh. Under adaptive refinement of the mesh based on a posteriori error estimation, output quantities of interest in the form of functionals of the finite element solution converge to become independent of the mesh resolution, and thus the resulting method has no adjustable parameters. No ad hoc design of the mesh is needed, instead the mesh is optimised based on solution features, in particular no bounder layer mesh is needed. We connect the computational method to the mathematical concept of a dissipative weak solution of the Euler equations, as a model of high Reynolds number turbulent flow, and we highlight a number of benchmark problems for which the method is validated.

*Keywords:* finite element method, adaptive mesh refinement, turbulent simulation
*2010 MSC:* 00-01, 99-00

## 1. Introduction

Turbulence is central for our understanding of the world, including the geophysical flow of the ocean-atmosphere system, and the aerodynamics of vehicles,

*Email address:* jhoffman@kth.se (Johan Hoffman)
*URL:* www.csc.kth.se/∼jhoffman (Johan Hoffman)

aircraft and wind turbines, for example. Simulation of turbulent flow is an outstanding problem that cuts through mathematics, numerical analysis, scientific computing and fluid mechanics. This interdisciplinary nature of the problem makes it particularly challenging.

In this paper we present our work towards a general framework for simulation of unsteady high Reynolds number turbulent flow using adaptive finite element methods based on adjoint analysis. We recall the theoretical foundation and show how this framework offers solutions to the main challenges of turbulence simulation: how to assess the accuracy in a simulation, how to minimise the dependency on application specific model parameters, and how to optimise the use of computational resources. To our best knowledge, application of adjoint based adaptive methods to simulate unsteady turbulent flow in 3D is still rare [1, 2]. The purpose of this paper is to give a coherent presentation of our computational framework, to report on recent progress, and to highlight challenges and open problems.

### *1.1. Turbulence simulation*

The fundamental mathematical model of fluid flow is the nonlinear Navier-Stokes equations in 3 space dimensions, for which a proof of existence of classical (smooth) solutions in the general case is missing. To compute approximate solutions of the Navier-Stokes equations in the case of turbulent flow is extremely expensive; an heuristic argument estimates the number of degrees of freedom needed to resolve all turbulent scales in a Direct Numerical Simulation (DNS) to be of the order $Re^{9/4}$, with $Re$ the Reynolds number, which for many decades to come will make DNS impossible e.g. for geophysical flow or flight aerodynamics where $Re >> 10^6$.

A reduction in the number of degrees of freedom is possible by instead considering models for averaged quantities, such as statistical mean fields in RANS (Reynolds averaged Navier-Stokes equations) or spatially filtered fields in LES (Large eddy simulation), at the cost of introducing turbulence/subgrid models to model unresolved statistical fluctuations/subgrid scales [3]. This *closure problem* of turbulence modelling has proven to be an outstanding problem, where model parameters often have to be tuned to a particular application. Similarly, subgrid models introduce parameters that need to be chosen by the user, in particular near solid walls it is a challenge to select proper parameters to accurately capture phenomena such as flow separation [4].

In RANS/LES simulations, the relation between model errors and numerical errors is delicate, since the effect of the numerical method often is similar to the effect of turbulence/subgrid models, e.g. in the form of dissipation of kinetic energy. For example, the widely used Smagorinsky subgrid model [5] is closely connected to methods of artificial viscosity used to stabilise numerical methods [6]. To tackle this issue, different approaches have been attempted, from using high order numerical methods with minimal dissipation, to interpreting the numerical stabilisation as the subgrid model [7, 8, 9, 10], or alternatively trying to balance the two sources of errors [11, 12]. The relationship between the local resolution of the computational mesh and the turbulent length scales of

RANS and LES also poses challenges, in particular near solid walls where small turbulent scales dictate a very fine mesh resolution which dominates the total computational cost [4].

In the context of finite element methods, Variational Multiscale Stabilized methods (VMS) [9] have been developed where the variational form of the Navier-Stokes equations is split into resolved scales and subgrid scales, by decomposing the underlying Hilbert space into a direct sum of a coarse space and a fine space, where a subgrid model is used to model the fine scale contribution.

### *1.2. Dissipative weak solutions*

In the framework presented in this paper we follow a different path, where we avoid the process of averaging and scale separation altogether, and thus also the closure problem. For incompressible flow the mathematician Jean Leray in 1934 [13] proved the existence of a *weak solution*, or turbulent solution (*solution turbulente*) in the terminology of Leray, that is a function that satisfies a weak form of the Navier-Stokes equations (in the sense of distributions). The work of Leray laid the foundation for the modern mathematical theory of the Navier-Stokes equations, and the regularised form of the equations used by Leray later inspired a specific class of LES methods [14]. The question of uniqueness of a weak solution is still an open problem, and whether a weak solution is also a smooth (strong) solution is formulated as a $1 million Clay Prize problem [15]. A weak solution does not satisfy the standard energy balance valid for a smooth solution of the Navier-Stokes equations, instead only an energy inequality can be shown to hold. Partial regularity of a weak solution was proven under the assumption that a generalised energy inequality holds [16, 17], in which case the weak solution is referred to as a *suitable weak solution*. It can be shown that many discrete approximations, including finite element approximations, converge to suitable solutions [18].

For a weak solution, dissipation without viscosity is possible. In particular, Duchon and Robert in 2000 introduced the notion of a *dissipative weak solution* as a model for high Reynolds number turbulent flow, where an explicit expression for the source of inviscid dissipation was derived, which took the form of a local lack of regularity in the velocity field [19]. Already in 1949, Onsager suggested that weak solutions of the inviscid Euler equations (assuming such exist) could be used to model high Reynolds number turbulent flow [20]:

*"It is of some interest to note that in principle, turbulent dissipation as described could take place just as readily without the final assistance by viscosity. In the absence of viscosity, the standard proof of the conservation of energy does not apply, because the velocity field does not remain differentiable!"*

A consequence of the idea that turbulent dissipation is independent of viscosity, is that it should be possible to model turbulence without any empirical parameters. Onsager also conjectured that in such "ideal" turbulence, the regularity of the velocity field could at most satisfy a Hölder condition with exponent 1/3, otherwise the energy would be conserved. Several proofs of Onsager's conjecture have since then been presented, and in their 2006 review of the work of

Onsager, Eyink and Sreenivasan end with a conclusion on the future of Onsagers ideas [21]:

*"We believe that Onsagers theoretical vision of an ideal turbulence described by inviscid fluid equations is a proper idealization for understanding high Reynolds number flows. Needless to say, in real physical turbulence there is viscosity, which is always positive. [...] In the same way, the zero-viscosity limit, which supposes an infinite number of cascade steps, should be a good idealization for turbulence with a large but finite number of cascade steps, that is, a Reynolds number which is large but finite. The vindication of this belief, if it is true, must come from a set of calculational tools for the zero-viscosity limit, which will make it, in the end, a truly predictive device."*

### *1.3. Direct finite element simulation*

In [8, 22, 23] we show that approximate dissipative weak solutions can be computed to simulate turbulent flow using a stabilised finite element method that satisfies certain conditions on stability and consistency, which we refer to as a *General Galerkin (G2) method*. We also refer to the computational methodology as *Direct Finite Element Simulation (DFS)*, as an extension to turbulent flow of the general framework of a posteriori error estimation developed in the early 1990s [24, 25]. In particular, for high Reynolds numbers we can set the viscosity to zero, thus realising a computational model of turbulent flow free from empirical parameters.

We argue that the proper mathematical objects for assessing well-posedness in DFS are functionals of the computed weak solutions [26]. To represent the error in a functional of a dissipative weak solution we introduce a dual (adjoint) linearised problem, which opens for a posteriori estimation of the error in outputs of interest, such as the drag and lift of an airplane. The a posteriori error representation can be used to construct efficient adaptive algorithms, where the computational mesh and the finite element space are optimised for the computation of a particular output of interest (goal functional) to a certain accuracy using minimal computational resources. Thus also the local resolution of turbulent scales is determined as part of the computation (a posteriori) based on what functional is the goal of the simulation. For example, approximation of the aeroacoustic sources in a turbulent flow past a landing gear may demand a different mesh resolution than approximation of the aerodynamic forces on the same landing gear [27, 28].

A classical problem of great significance is the prediction of aerodynamic forces acting on a body in a high Reynolds number flow. The choice of boundary conditions in the simulation is here central. As already noted, for realistic applications e.g. in flight aerodynamics, full resolution of a turbulent boundary layer in DNS is impossible due to the computational cost. In LES, typical models of the near wall turbulent flow are wall shear stress models [4] or local RANS models near the wall [29], where both approaches demand high resolution boundary layer meshes and calibration of model parameters.

In [30] we investigate a simple wall shear stress model parametrised by the skin friction stress generated by the turbulent boundary layer. We find that for very high Reynolds numbers, corresponding to small skin friction, the macroscopic flow is largely independent of the wall shear stress model. In particular, the skin friction parameter can be set to zero, corresponding to a free slip boundary condition, and no boundary layer mesh is needed. For high Reynolds number flow, DFS with a free slip boundary condition has been shown to be an efficient and accurate model for approximation of aerodynamic forces and aeroacoustic sources [27, 28, 31, 32].

In this paper we describe the DFS framework for incompressible turbulent flow, and we report on recent work to validate the method. The G2/DFS framework is presented in Section 2, and we give a brief description of a detailed implementation of the method in Section 3. In Section 4 we report on validation studies for the computational model, in Section 5 we discuss stability and computability of turbulent flow, and in Section 6 we give a short summary.

## 2. The G2/DFS computational framework

Low Mach number flow can be approximated by incompressible flow, and the focus of this paper is the model of incompressible high Reynolds number turbulent flow around bluff or streamlined bodies, where the Reynolds number is defined as $Re = \frac{UL}{\nu}$, with $U$ a characteristic velocity, $L$ a characteristic length and $\nu$ is the kinematic viscosity.

### *2.1. Mathematical model*

The Navier-Stokes equations for incompressible flow of (small positive) constant kinematic viscosity $\nu$ in a (bounded) volume $\Omega$ in $\mathbf{R}^3$ around a fixed rigid body with smooth boundary $\Gamma$ over a time interval $I = [0, T]$, take the form: Find the velocity $u = (u_1, u_2, u_3)$ and pressure $p$ depending on $(x, t) \in \Omega \cup \Gamma \times I$, such that

$$\begin{aligned} \dot{u} + (u \cdot \nabla)u + \nabla p - \nabla \cdot \tau &= 0 && \text{in } \Omega \times I, \\ \nabla \cdot u &= 0 && \text{in } \Omega \times I, \\ u_n &= 0 && \text{on } \Gamma \times I, \\ \tau_{s_k} &= \beta u_{t_k} && \text{on } \Gamma \times I, \\ u(\cdot, 0) &= u^0 && \text{in } \Omega, \end{aligned} \tag{1}$$

with $k = 1, 2$, $\dot{u} = \frac{\partial u}{\partial t}$, $u_n = u \cdot n$ the fluid velocity normal to $\Gamma$ with $n$ a unit outward normal vector, $\tau = \tau(u) = 2\nu\epsilon(u)$ the viscous stress with $\epsilon(u)$ the standard velocity strain, $\tau_{s_k}$ the tangential stresses and $u_{t_k} = u \cdot t_k$ the tangential velocities with $t_k$ orthogonal tangent vectors, and $u^0$ a given initial condition.

We assume suitable far-field inflow/outflow boundary conditions, and we note the Dirichlet-Neumann boundary condition in the normal and tangential directions, respectively, with the effect of turbulent boundary layers modeled by

a (skin) friction parameter $\beta$. With zero viscosity $\nu$ and boundary friction $\beta$, the model (1) reduces to the inviscid Euler equations.

In [19] it is shown that for any weak solution $(u, p)$ of the Euler equations (assumed to exist), a local energy equation is satisfied

$$\frac{d}{dt}(\frac{1}{2}|u|^2) + \nabla \cdot (u(\frac{1}{2}|u|^2 + p)) + D(u) = 0, \tag{2}$$

with $D(u)$ defined in terms of the local smoothness of $u$. If $D(u) \geq 0$, then $(u, p)$ is referred to as a dissipative weak solution.

### *2.2. Finite element method*

In G2/DFS we compute approximate solutions of the Navier-Stokes equations (1) by a weighted residual stabilized finite element method, of the form: Find $\hat{U} = (U, P) \in V_h$ such that for all $\hat{v} = (v, q) \in V_h$

$$[R(U; \hat{U}), \hat{v}] + [hR(U; \hat{U}), R(U; \hat{v})] = 0, \tag{3}$$

where $V_h$ is a space-time finite element space with velocities $v$ satisfying $v \cdot n = 0$ on $\Gamma$, $[\cdot, \cdot]$ is an $L_2(\Omega \times I)$ inner product, $R(U; \hat{v}) = (\dot{v} + U \cdot \nabla v + \nabla q, \nabla \cdot v)$ is the residual, and $h$ is the local mesh size. The first term in (3) establishes $\hat{U}$ as a weak solution of (1) and the second term introduces kinetic energy dissipation $D_h(\hat{U}) = [hR(U; \hat{U}), R(U; \hat{U})] = \|h^{0.5} R(U; \hat{U})\|^2_{L_2}$ bounded by data with $\|\cdot\|_{L_2}$ an $L_2(\Omega \times I)$ norm [22].

Notice that here $\nu$ and $\beta$ are set to zero with instead the weighted residual stabilization introducing a dissipative effect as an automatic turbulence model. This is analogous to the dissipative weak solutions introduced by Duchon and Robert [19], with dissipation caused by a lack of smoothness in the velocity field, unrelated to viscous dissipation. For a smooth solution $\hat{U}$, corresponding to a small residual in $L_2(\Omega \times I)$, the dissipative effect of the weighted residual stabilization vanishes. In Section 4 we report on validation results showing that DFS based on the Euler equations is a good approximation of high Reynolds number turbulent flow. We also find that with sufficient mesh resolution, $D_h(\hat{U})$ is independent of the local mesh size $h$ [23].

In Section 3 we give a precise definition of a particular implementation of G2/DFS, but many choices are possible as long as certain conditions for stability and consistency are satisfied [22, 23].

### *2.3. Boundary conditions*

It is well known that for viscous flow, thin boundary layers develop near solid walls over which the velocity changes from the velocity of the wall to the free stream velocity. The thickness of these boundary layers scale with the Reynolds number, and at high Reynolds numbers the boundary layers are so thin that computational resolution is impractical or impossible. At sufficiently high Reynolds numbers the boundary layers undergo transition to turbulence, where computational resolution of turbulent boundary layers is even less realistic

in any application of significance [4]. For example, full computational resolution in DNS of the turbulent flow around a car or an airplane, including boundary layers, is impossible for many years to come [33].

Ever since the introduction of the boundary layer concept by Prandtl [34], models of the flow decoupling the boundary layer from the interior flow have been pursued, in which the effect of the boundary layer is modelled as a boundary condition for the interior flow [4]. In (1) we model the effect of turbulent boundary layers as a small skin friction stress at the solid boundary, which dissipates kinetic energy proportional to $\beta$. The sensitivity of the solution with respect to perturbations in the skin friction parameter $\beta$ is investigated in [35, 30], where it is found that for small $\beta$ (corresponding to high Reynolds numbers) the sensitivity is low. In particular, for external flow at Reynolds numbers higher than $Re > 10^6$ we typically approximate the small skin friction by zero, which makes DFS into a parameter-free model of high Reynolds number external flow.

We have presented evidence in the form of analysis and computational studies, that for high Reynolds numbers the macroscopic flow, including 3D flow separation, is mainly determined by large scale stability aspects, rather than boundary layer effects [36, 27, 28, 31, 32].

### *2.4. A posteriori error estimation*

The goal of a simulation can often be formulated as computing a number of output quantities, for example the lift and drag of an airplane. To estimate the error in an output functional of interest we follow the general framework for a posteriori error analysis based on sensitivity information from the solution of a dual (adjoint) problem, developed in the 1990s [24, 25, 37]. In [38, 12, 8, 39] we extended this framework to a posteriori error estimation of turbulent flow, validated for basic model problems as well as for challenging benchmark problems in complex geometry.

We define a target functional $M(\hat{u}) = [\hat{u}, \hat{\psi}] + [pn, \psi_\Gamma]_\Gamma$, where $\hat{\psi} = (\psi, \chi)$ is a given weight function acting as data for the dual problem, and $\psi_\Gamma$ is boundary data for the dual velocity, with $[\cdot,\cdot]_\Gamma$ a $L_2(\Gamma \times I)$ inner product. To choose the lift and drag of an airplane as the target functional we set $\hat{\psi} = 0$ and $\psi_\Gamma = v_D + v_L$, with $v_D$ and $v_L$ unit vectors in directions opposite and normal to the flight direction, respectively.

The difference in output $M(\hat{u}) - M(\hat{U}) = [\hat{u}, \hat{\psi}] + [pn, \psi_\Gamma]_\Gamma - [\hat{U}, \hat{\psi}] - [Pn, \psi_\Gamma]_\Gamma$ of two DFS solutions $\hat{u}$ and $\hat{U}$ on different meshes with maximal mesh size $h$, can be represented as

$$M(\hat{u}) - M(\hat{U}) = [R(u;\hat{u}) - R(U;\hat{U}), \hat{\varphi}] \tag{4}$$

where $\hat{\varphi} = (\varphi, \theta)$ is a solution of the dual linearized problem

$$\begin{array}{rcll} -\dot{\varphi} - (u\cdot\nabla)\varphi + \nabla U^T\varphi + \nabla\theta &=& \psi & \text{in } \Omega\times I,\\ \nabla\cdot\varphi &=& \chi & \text{in } \Omega\times I,\\ \varphi &=& \psi_\Gamma & \text{on } \Gamma\times I,\\ \varphi(\cdot,T) &=& 0 & \text{in } \Omega, \end{array} \tag{5}$$

where $(\nabla U^T \varphi)_j = \sum_{i=1}^3 \partial U_i/\partial x_j \varphi_i$.

If we assume that the time step is bounded by $h$, we can bound the output error using basic analysis [22]:

$$|M(\hat{u}) - M(\hat{U})| \leq C\|h^{0.5}\hat{\varphi}\|_{H^1}, \tag{6}$$

with a constant $C$ depending on data and bounds on the magnitude of the discrete velocities $u$ and $U$. We thus have stability in output if $\|h^{0.5}\hat{\varphi}\|_{H^1}$ is small, where $H^1 = H^1(\Omega \times I)$ is the standard Hilbert space with associated norm.

### *2.5. Adaptive algorithm*

A posteriori error estimation provides a powerful tool for the development of robust and efficient adaptive algorithms. The basic idea of adaptive algorithms is to optimize the computational method with respect to the goal (output of interest) of the computation. Typical parameters of an adaptive finite element method include the local mesh size (h-adaptivity), local degree of the finite element approximation (p-adaptivity), local shape of the cells (r-adaptivity), or combinations thereof.

We here focus on h-adaptivity. To construct an adaptive algorithm we compute a DFS solution $\hat{U}$ for which we use the error representation (4) to estimate the output error $|M(\hat{u}) - M(\hat{U})|$, with $\hat{u}$ any DFS solution computed on a finer mesh than $\hat{U}$. We can either choose $\hat{u}$ and $\hat{U}$ to be two DFS solutions computed on different meshes in the mesh hierarchy generated by the adaptive algorithm, or alternatively to consider $\hat{u}$ to be an ideal solution computed on a finest mesh possible in which case we use the approximation $u \approx U$ in the dual problem (5).

An adaptive algorithm is based on an estimate of the local contribution to the global error, which is obtained by splitting the error representation (4) into a sum of *error indicators* $\mathcal{E}_{n,K}$ over the cells $K$ in the discrete space mesh $\mathcal{T}^h$, and the time intervals $I_n = (t_{n-1}, t_n)$, $n = 1, ..., N$, that is

$$M(\hat{u}) - M(\hat{U}) = \sum_{n=1}^{N} \sum_{K \in \mathcal{T}^h} \mathcal{E}_{n,K} = \sum_{n=1}^{N} \sum_{K \in \mathcal{T}^h} [R(u;\hat{u}) - R(U;\hat{U}), \hat{\varphi}]_{n,K} \tag{7}$$

with $[\cdot,\cdot]_{n,K}$ an $L_2(K \times I_n)$ inner product.

One basic adaptive algorithm is to keep the mesh constant in time and then iteratively refine an initial mesh based on (7) until convergence in $M(\hat{U})$ is observed.

Adaptive algorithm: given initial coarse mesh $\mathcal{T}_0^h$, $k = 0$,

(1) compute solution to primal problem using $\mathcal{T}_k^h$
(2) compute solution to dual problem using $\mathcal{T}_k^h$
(3) if convergence in $M(\hat{U})$ is observed, or if the estimated error based on (4) is less than the tolerance, then STOP, else
(4) refine a fixed fraction of cells in $\mathcal{T}_k^h$ with largest contribution to the error based on (7)
(5) set $k = k + 1$, then goto (1)

### 2.6. Approximation of the dual solution

There are several technical aspects with respect to how to apply the error representation formula (7), in particular with regards to the approximation of $\hat{\varphi}$, the solution to the dual problem.

The dual problem is linear, but runs backward in time which is a challenge since the DFS velocities $u$ and $U$ act as coefficients in the dual problem and thus have to be stored as data. In practise, the dual problem is solved using a similar finite element method as used for the primal DFS problem, and the coefficients $u$ and $U$ can be interpolated in time to minimize data storage, with possibly a restart scheme to increase accuracy. Also, several different approaches are possible for how to apply the error representation formula (4) in practise [40], to retain sharpness and achieve maximal robustness.

When we use the approximation $u \approx U$ in the dual problem we introduce a linearization error which is hard to estimate a priori, since worst case estimates based on Gröwall's inequality grossly overestimate the effect [22]. In practice, computations on a sequence of meshes with different associated approximations $U$ provide an estimate of the asymptotic effect of this linearization error on the resulting a posteriori error estimates.

More specifically, the accuracy in the a posteriori error estimates depends on the accuracy in the approximation of the dual problem, which is affected by (i) perturbations in data and (ii) computational approximation. As part of the adaptive algorithm, approximations of the dual problem are computed on a hierarchy of computational meshes, which provides a robustness test with respect to (i)-(ii), improving the reliability of the a posteriori error estimates.

## 3. DFS implementation

We now give a detailed presentation of an implementation of DFS, in the form of the cG(1)cG(1) method with piecewise linear approximation in space and time over tetrahedral meshes. In Section 4 we report on validation studies of this method.

### 3.1. The cG(1)cG(1) method

The cG(1)cG(1) method is based on the continuous Galerkin method cG(1) in space and time. With cG(1) in time the trial functions are continuous piecewise linear and the test functions piecewise constant. cG(1) in space corresponds to both test functions and trial functions being continuous piecewise linear. Let $0 = t_0 < t_1 < ... < t_N = T$ be a sequence of discrete time steps with associated time intervals $I_n = (t_{n-1}, t_n)$ of length $k_n = t_n - t_{n-1}$ and space-time slabs $S_n = \Omega \times I_n$, and let $W \subset H^1(\Omega)$ be a finite element space consisting of continuous piecewise linear functions on a tetrahedral mesh $\mathcal{T}^h$ of mesh size $h(x)$ with $W_0$ the functions $v \in W$ satisfying the Dirichlet boundary condition $v \cdot n|_\Gamma = 0$.

We seek $\hat{U} = (U, P)$, continuous piecewise linear in space and time: For $n = 1, ..., N$, find $(U^n, P^n) \equiv (U(t_n), P(t_n))$ with $U^n \in V_0^n \equiv [W_0]^3$ and $P^n \in W$,

such that

$$\begin{aligned}((U^n - U^{n-1})k_n^{-1} + \bar{U}^n \cdot \nabla \bar{U}^n, v) - (P^n, \nabla \cdot v) + (\nabla \cdot \bar{U}^n, q) \\ + SD_\delta^n(\bar{U}^n, P^n; v, q) = 0 \quad \forall \hat{v} = (v, q) \in V_0^n \times W^n,\end{aligned} \tag{8}$$

where $\bar{U}^n = \frac{1}{2}(U^n + U^{n-1})$ and $P^n$ are piecewise constant in time over $I_n$, with the stabilizing term

$$\begin{aligned}SD_\delta^n(\bar{U}^n, P^n; v, q) \equiv \\ (\delta_1(\bar{U}^n \cdot \nabla \bar{U}^n + \nabla P^n), \bar{U}^n \cdot \nabla v + \nabla q) + (\delta_2 \nabla \cdot \bar{U}^n, \nabla \cdot v),\end{aligned} \tag{9}$$

and

$$(v, w) = \sum_{K \in \mathcal{T}^h} \int_K v \cdot w \, dx,$$

with the stabilization parameters $\delta_1 = \kappa_1(k_n^{-2} + |U^{n-1}|^2 h^{-2})^{-1/2}$ and $\delta_2 = \kappa_2 h |U^{n-1}|$, where $\kappa_1$ and $\kappa_2$ are positive constants of unit size. We choose a time step size $k_n = C_{CFL} \min_{x \in \Omega} h/|U^{n-1}|$, with $C_{CFL}$ a constant of unit size.

**Remark 1.** *The cG(1) discretisation in time does not allow for a fully consistent stabilisation of the method, since the velocity test functions are constant in time. To make the method fully consistent while keeping a least squares stabilisation of the residual, we would need to use test functions that are linear discontinuous in time, corresponding to a cG(1)dG(1) method. The main reason for using cG(1)cG(1) is the reduction of the number of degrees of freedom by a factor 2.*

*3.2. cG(1)cG(1) energy equation*

We now recall that a cG(1)cG(1) solution satisfies a local energy equation, with dissipation directly proportional to the local residual. The proof is given in [23], so here the result is just stated. We define a family of smooth positive test functions $\phi_n(x)$ for $n = 1, ..., N$, with local compact support *supp* $\phi_n \subset \Omega$, and we define a piecewise constant function in time defined by $\phi(x, t) = \phi_n(x)$ for $t \in I_n$, normalized such that

$$\sum_{n=1}^N \int_\Omega \phi_n(x) \; dx \; k_n = 1.$$

**Theorem 2.** *Noting that $\delta_i \leq Ch$, for $i = 1, 2$, we have the following local energy estimate for cG(1)cG(1):*

$$\begin{aligned}&| \sum_{n=1}^N \; [ \; \int_\Omega (\frac{1}{2}(|U^n|^2 - |U^{n-1}|^2)k_n^{-1} + \nabla \cdot (\bar{U}^n(\frac{1}{2}|\bar{U}^n|^2 + P^n)))\phi_n \; dx \; ] \; k_n \\ &+ \sum_{n=1}^N \; [ \; \int_\Omega (\delta_1 |\bar{R}_1(\bar{U}^n, P^n)|^2 + \delta_2 |\bar{R}_2(\bar{U}^n)|^2)\phi_n \; dx \; ] \; k_n \; | \\ &\leq C h_{max,\phi,n}^{1/2}\end{aligned}$$

*with* $h_{max,\phi,n} \equiv \max_{n:supp\ \phi_n \neq \emptyset} (\max_{x \in supp\ \phi_n} h(x))$*, and with the residuals* $\bar{R}_1(\bar{U}^n, P^n)$ *and* $\bar{R}_2(\bar{U}^n)$ *defined by*

$$\bar{R}_1(v,q) = \dot{v} + \bar{U}^n \cdot \nabla v + \nabla q, \tag{10}$$

$$\bar{R}_2(v,q) = \nabla \cdot v, \tag{11}$$

*for* $t \in I_n$*.*

If we choose a test function $\phi$ with a suitable local support, and with $\phi_j = 0$ for all $j \neq n$, Theorem 2 states that for $t \in I_n$, a cG(1)cG(1) solution up to the factor $Ch^{1/2}_{max,\phi,n}$ weakly satisfies (integrated against of smooth positive test function with local support) a local energy equation of the form:

$$\frac{d}{dt}(\frac{1}{2}|U^n|^2) + \nabla \cdot (\bar{U}^n(\frac{1}{2}|\bar{U}^n|^2 + P^n)) = -D^n_h(\hat{U}), \tag{12}$$

with $D^n_h(\hat{U}) \equiv \delta_1 |\bar{R}_1(\bar{U}^n, P^n)|^2 + \delta_2 |\bar{R}_2(\bar{U}^n)|^2 \geq 0$, a residual based numerical dissipation.

This local energy equation connects to a dissipative weak Euler solution [19], with inertial energy dissipation coming from local non-smoothness of the solution, and not from any viscosity. The dissipative term $D^n_h(\hat{U})$ in (12) reflects local non-smoothness in the solution identified by the residuals, and is observed to be independent of $h$ under sufficient mesh resolution [39, 23]

*3.3. A posteriori error analysis and adaptive mesh refinement*

Using standard techniques of a posteriori error analysis, see e.g. [22], we can derive an a posteriori error estimate for cG(1)cG(1).

**Theorem 3.** *If* $\hat{U} = (U, P)$ *solves (8),* $\hat{u} = (u, p)$ *is a weak solution to (1), and* $\hat{\varphi} = (\varphi, \theta)$ *solves (5), then we have the following a posteriori error estimate for the output* $M(\hat{U}) = [\hat{U}, \hat{\psi}]$ *with respect to the reference output* $M(\hat{u}) = [\hat{u}, \hat{\psi}]$*:*

$$|M(\hat{u}) - M(\hat{U})| \leq \sum_{n=1}^{N} [ \int_{I_n} \sum_{K \in \mathcal{T}^h} |R_1(\hat{U})|_K \cdot \omega_1 \ dt$$
$$+ \int_{I_n} \sum_{K \in \mathcal{T}^h} |R_2(U)|_K \ \omega_2 \ dt + \int_{I_n} \sum_{K \in \mathcal{T}^h} |SD^n_\delta(\hat{U}; \hat{\varphi})_K| \ dt \ ]$$

*with*

$$R_1(\hat{U}) = \dot{U} + (U \cdot \nabla)U + \nabla P,$$
$$R_2(U) = \nabla \cdot U,$$

*where* $SD^n_\delta(\cdot;\cdot)_K$ *is a local version of the stabilizing form (9), and the stability weights are given by*

$$\omega_1 = C^k_{n,K} k_n |\dot{\varphi}|_{K,\infty} + C^h_{n,K} h_K |\nabla \varphi|_K,$$
$$\omega_2 = C^k_{n,K} k_n |\dot{\theta}|_{K,\infty} + C^h_{n,K} h_K |\nabla \theta|_K,$$

*where $h_K$ is the diameter of element $K$ in the mesh $\mathcal{T}^h$, $C^h_{n,K}, C^k_{n,K}$ represent interpolation constants, $|w|_K \equiv (\|w_1\|_K, \|w_2\|_K, \|w_3\|_K)$ with $\|w\|_K = (w,w)^{1/2}_K$, and the dot denotes the scalar product in $\mathbb{R}^3$.*

### *3.4. Software implementation*

The adaptive algorithm and the cG(1)cG(1) solver is implemented in the unified continuum mechanics solver Unicorn [41] and the high performance (HPC) branch of the finite element problem solving environment DOLFIN, part of the FEniCS project [42]. The HPC branch of DOLFIN [43, 44] is optimized for distributed memory architectures using a hybrid MPI+OpenMP approach with efficient parallel I/O (MPI I/O), and ParMETIS [45] is used for mesh partitioning. DOLFIN supports several parallel linear algebra packages, but mostly rely on PETSc [46].

## 4. Validation and application of DFS

DFS is based on the computation of finite element approximations on adaptively refined computational meshes. In particular, no ad hoc mesh design is needed, since solutions features such as flow separation and turbulent wakes are automatically detected by the adaptive method through a posteriori error estimation with sensitivity information from the solution of a dual problem. A hierarchy of adaptively refined meshes is generated for which convergence can be observed with respect to an output of interest. We now report on the validation of DFS in the form of the cG(1)cG(1) method.

### *4.1. Medium Reynolds number flow*

At medium Reynolds numbers, less than $Re = 10^5$, boundary layers are laminar and can be resolved by the computational mesh. For this case, viscous effects are not negligible so that the viscosity is kept in the model (1), and no slip boundary conditions are chosen where the velocity is set to zero on the solid boundary $\Gamma$.

DFS in the form of the cG(1)cG(1) method has been validated for a number of model problems of simple geometry bluff bodies, including a surface mounted cube and a rectangular cylinder [39, 8], a sphere [47] and a circular cylinder [48]. In each case, convergence is observed for output quantities such as drag, lift and pressure coefficients, and Strouhal numbers, and the adaptive algorithm leads to an efficient method often using orders of magnitude fewer number of degrees of freedom compared to LES methods based on ad hoc design of the mesh.

### *4.2. High Reynolds number flow*

In high Reynolds number flow, with $Re > 10^6$, boundary layers are turbulent and are in most cases too expensive to resolve, and must instead be modeled. To accurately predict e.g. aerodynamic forces it is critical to capture the correct flow separation, which can be connected to the boundary layer, in case flow separation is not triggered by sharp features in the geometry [23]. Drag crisis

for a circular cylinder is an illustrative example, where flow separation moves downstream the cylinder wall as a consequence of transition to turbulence in the boundary layer [49]. In [30] we model drag crisis by decreasing the skin friction parameter $\beta$ in the model (1), where we find that the DFS simulations reproduce the observed drag crisis scenario from experiments [50, 51, 52, 53].

In particular, we find that for small $\beta$ the solution is insensitive to the particular value of $\beta$, so that we reach an ultimate regime where the turbulent boundary layer is modeled by a zero friction free slip boundary condition. This free slip model has the benefit of being a parameter-free model of turbulent boundary layers, which requires no boundary layer mesh since no boundary layer is resolved. For a high Reynolds number, the free slip boundary condition has been shown to be a good model in the sense that flow separation and thereby the surface pressure distribution is well approximated. For high Reynolds numbers, the main contribution to the aerodynamic forces on a body comes from the surface pressure distribution, and thus the free slip model has a high potential in aerodynamics applications.

DFS with a free slip boundary condition has been validated for the standard benchmarks of a NACA 0012 wing [54] and a 30P30N high lift device [55], where close agreement with experimental measurement was found in aerodynamic forces and surface pressure distribution.

### *4.3. Complex geometry*

To assess the capability of DFS for more challenging high Reynolds number flow problems in complex geometry, we have participated in a number of benchmark workshops with detailed experimental data available for validation, including the first and second workshops on *Benchmark problems for Airframe Noise Computations* (BANC-I and BANC-II) [28, 31], and the *2nd AIAA CFD High Lift Prediction Workshop* (HiLiftPW-2) [32].

Good agreement was found between DFS simulations and experimental measurements in all workshops, and two features distinguished DFS from all other methodologies: (i) DFS was the only method using adaptive mesh optimisation, and (ii) DFS was the only method leaving boundary layers unresolved (free slip boundary conditions were used for all problems). Both (i) and (ii) contributed to the fact that the number of degrees of freedom used in DFS was significantly lower than in other methods, often several magnitudes less.

In HiLiftPW-2 the task was to simulate flow at high Reynolds number around a full aircraft, where DFS was the only method based on Navier-Stokes equations that simulated the unsteady flow [32]; aside from 2 contributions based on Lattice Boltzmann Methods all other contributions used stationary RANS. Good agreement of DFS simulations and experimental data was found in aerodynamic forces and surface pressure distributions on the wings, see Fig. 1-4, and the transient simulation data provided additional data on the flow at high angles of attack modelling take-off and landing.

We note that the only input data to the DFS model is the geometry of the airplane, in the form of an initial coarse mesh, since viscosity and skin friction are assumed to be negligible.

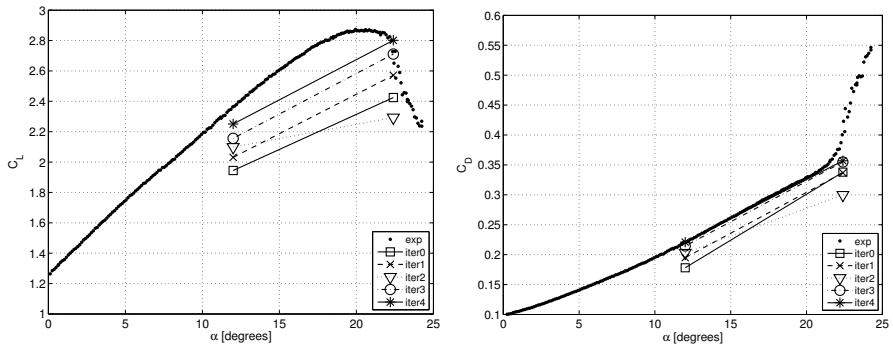


Figure 1: From [32]: Lift and drag coefficient for angles of attack 12° and 22.4°, under adaptive mesh refinement with the computational approximations approaching the experimental reference values.

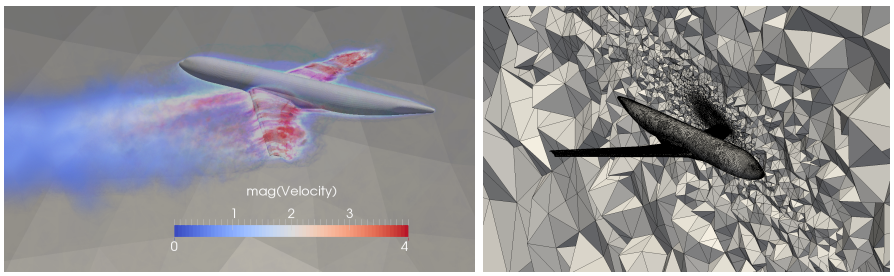


Figure 2: From [32]: Snapshot of the magnitude of dual velocity (left), and an adaptively refined computational mesh optimised for lift and drag approximation (right).

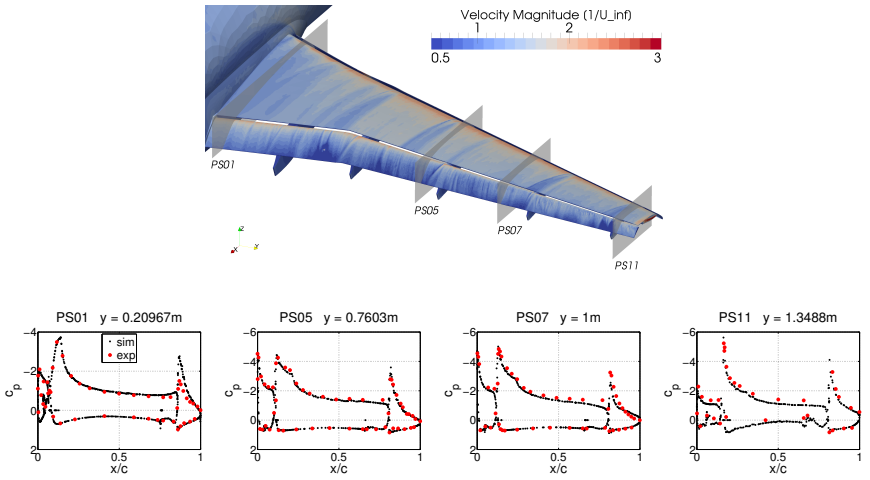


Figure 3: From [32]: Mean velocity contours and measurement plane locations (upper), and pressure coefficient, $C_P$, vs. normalized local chord, $x/c$, (lower) for the angle of attack $\alpha = 12^o$, for a complete wing-body configuration.

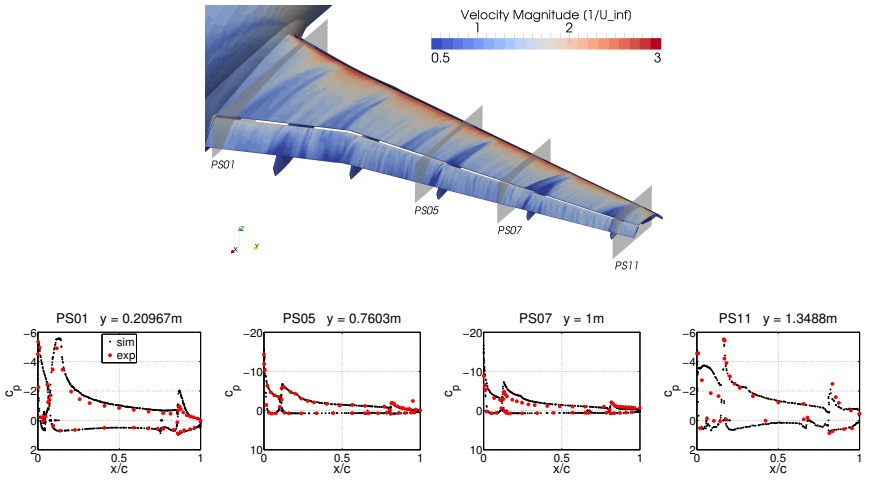


Figure 4: From [32]: Mean velocity contours and measurement plane locations (upper), and pressure coefficient, $C_P$, vs. normalized local chord, $x/c$, (lower) for the angle of attack $\alpha = 22.4^o$, for a complete wing-body configuration.

## 5. Stability and computability of turbulent flow

Characteristic for turbulent flow are chaotic particle paths which make prediction of point values hard or impossible, popularly referred to as the butterfly effect. But turbulence is also a dissipative mechanism, similar to a shock in high Mach number flow, with many stable features in the sense of averages, which is what makes turbulence simulation possible. For example, although the particular set of particle paths around an airplane is impossible to predict, the net effect in terms of the time average of aerodynamic forces is a stable quantity.

### *5.1. Stability of the dual problem*

Particle paths in a turbulence simulation are chaotic, but mean value output can be stable. The difference between two computed solutions $\hat{u}$ and $\hat{U}$ with respect to an output functional $M(\cdot)$ can be expressed as the duality pairing of local residual errors with the solution of a dual (adjoint) problem linearised at the two computed solutions, which is the posteriori error representation (4) that is the foundation of the DFS adaptive method. In particular, the computational approximation of the dual solution is at the heart of the methodology, and thus the well-posedness of the dual problem is critical: is the dual problem solvable, and what is the sensitivity in the dual solution with respect to its data (the linearisation error)?

A worst case case analytical estimate using Grönwall's inequality bounds the dual solution in terms of rapid exponential growth in time [22], although in practise approximations of the dual solution for turbulent flow is routinely computed as part of the DFS method. Practical computation also shows that the dual solution is stable with respect to different data in the form of approximate primal solutions. That is, when the computational mesh is sufficiently refined so that the output functional of interest $M(\hat{U})$ (e.g. drag) has converged, little difference is seen in dual solutions $\hat{\varphi}$ linearised at different approximate solutions $\hat{U}$ from this class of approximate solutions, which is observed as part of the adaptive algorithm [22].

The dual equations is a system of convection-reaction equations that take the gradient $\nabla U$ as reaction coefficient. Given the sharp gradients in turbulent flow, how is well-posedness of the dual problem possible? In [22] we argue that the key is cancellation, since in a turbulent flow the gradient is oscillating rapidly, so that exponential growth is alternating with exponential decay. In particular, a turbulent wake is dominated by vortices on a range of scales, see Fig. 5, where each individual vortex tube is a stable flow structure in the sense that a linearised stability analysis show no exponential perturbation growth [22].

### *5.2. Blowup of the dual solution*

On the other hand, there are unstable flows which are highly sensitive to perturbations, for which blowup in the dual solution has been observed. An illustrative example is flow around a circular cylinder, where as the Reynolds

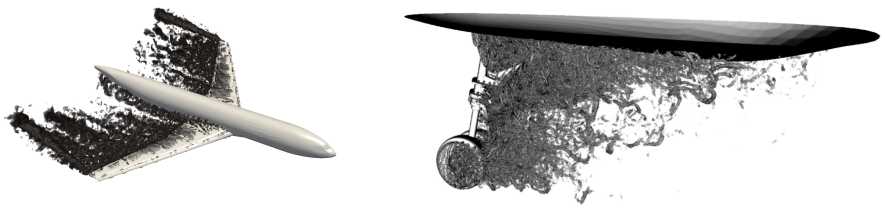

Figure 5: Vorticity visualised by a Q-criterion: snapshot of a DFS solution of the flow around of a wing-body configuration (left) [32], and flow around a Gulfstream G550 nose landing gear (right) [31].

number increases, the flow undergoes bifurcations connected to the first development of 3D flow features, then transition to turbulence in shear layers, wakes and boundary layers [49].

In particular, observations of blowup in the dual solution have been reported for increasing Reynolds numbers in the case of 2D flow around a circular cylinder [56, 57], with strong vorticity production resulting from a sharpening of the boundary layers and without any mechanism for dissipation in 2D. In physical flow, 3D features and turbulens develop that dissipate vorticity through vortex stretching, which can be observed in corresponding 3D simulations [48].

## 6. Summary

We have presented a computational framework for turbulence simulation based on adaptive finite element approximation, which we refer to as Direct Finite Element Simulation (DFS). For high Reynolds numbers, viscosity and wall shear stress are assumed to be negligible compared to inertial effects, and thus the DFS model has no empirical parameters. We interpret a DFS approximation as a dissipative weak solution, for which we can estimate the error with respect to output functionals using duality analysis.

Validation of the method has been carried out for a number of benchmark problems, where it is found that DFS simulations compare well with experimental data, while at the same time being a very efficient methodology in terms of the number of degrees of freedom needed to compute output data such as aerodynamics forces and surface pressure distributions. The main distinguishing features of the parameter-free version of DFS are: (i) the computational mesh is optimised based on a goal functional using a posteriori error estimation, and (ii) turbulent boundary layers are left unresolved.

## Acknowledgements

The author would like to thank Johan Jansson, Niclas Jansson and Rodrigo Vilela De Abreu who generously contributed images to this paper.

The author also acknowledge the financial support from the Swedish Foundation for Strategic Research, the European Research Council, and the Swedish Research Council. The simulations were performed on resources provided by the Swedish National Infrastructure for Computing (SNIC) at PDC – Center for High-Performance Computing, and the Barcelona Supercomputing Center - Centro Nacional de Supercomputacion.

## References

[1] K. J. Fidkowski, D. L. Darmofal, Review of output-based error estimation and mesh adaptation in computational fluid dynamics, AIAA journal 49 (4) (2011) 673–694.

[2] J. Slingo, K. Bates, N. Nikiforakis, M. Piggott, M. Roberts, L. Shaffrey, I. Stevens, P. L. Vidale, H. Weller, Developing the next-generation climate system models: challenges and achievements, Philosophical Transactions of the Royal Society A: Mathematical, Physical and Engineering Sciences 367 (1890) (2009) 815–831. arXiv:http://rsta.royalsocietypublishing.org/content/367/1890/815.full.pdf+html, doi:10.1098/rsta.2008.0207.
URL http://rsta.royalsocietypublishing.org/content/367/1890/815.abstract

[3] P. Sagaut, Large eddy simulation for incompressible flows, 3rd edition, Springer, 2005.

[4] U. Piomelli, E. Balaras, Wall-layer models for large-eddy simulations, Annual review of fluid mechanics 34 (1) (2002) 349–374.

[5] J. Smagorinsky, General circulation experiments with the primitive equations: I. the basic experiment*, Monthly weather review 91 (3) (1963) 99–164.

[6] J. VonNeumann, R. D. Richtmyer, A method for the numerical calculation of hydrodynamic shocks, Journal of Applied Physics 21 (3) (1950) 232–237. doi:http://dx.doi.org/10.1063/1.1699639.
URL http://scitation.aip.org/content/aip/journal/jap/21/3/10.1063/1.1699639

[7] C. Fureby, F. Grinstein, Monotonically integrated large eddy simulation of free shear flows, AIAA journal 37 (5) (1999) 544–556.

[8] J. Hoffman, C. Johnson, A new approach to computational turbulence modeling, Computer Methods in Applied Mechanics and Engineering 195 (23) (2006) 2865–2880.

[9] Y. Bazilevs, V. Calo, J. Cottrell, T. Hughes, A. Reali, G. Scovazzi, Variational multiscale residual-based turbulence modeling for large eddy simulation of incompressible flows, Computer Methods in Applied Mechanics and Engineering 197 (1) (2007) 173–201.

[10] J. Principe, R. Codina, F. Henke, The dissipative structure of variational multiscale methods for incompressible flows, Computer Methods in Applied Mechanics and Engineering 199 (13) (2010) 791–801.

[11] J. Meyers, B. Geurts, P. Sagaut, A computational error-assessment of central finite-volume discretizations in large-eddy simulation using a smagorinsky model, Journal of Computational Physics 227 (1) (2007) 156–173.

[12] J. Hoffman, On duality-based a posteriori error estimation in various norms and linear functionals for large eddy simulation, SIAM Journal on Scientific Computing 26 (1) (2004) 178–195.

[13] J. Leray, Sur le mouvement d'un liquide visqueux emplissant l'espace, Acta mathematica 63 (1) (1934) 193–248.

[14] J. Guermond, J. Oden, S. Prudhomme, An interpretation of the navier–stokes-alpha model as a frame-indifferent leray regularization, Physica D: Nonlinear Phenomena 177 (1) (2003) 23–30.

[15] C. Fefferman, Official clay prize problem description: Existence and smoothness of the navier-stokes equation (2000).

[16] V. Scheffer, et al., Partial regularity of solutions to the navier-stokes equations, Pacific J. Math 66 (2) (1976) 535–552.

[17] L. Caffarelli, R. Kohn, L. Nirenberg, Partial regularity of suitable weak solutions of the navier-stokes equations, Communications on pure and applied mathematics 35 (6) (1982) 771–831.

[18] J.-L. Guermond, On the use of the notion of suitable weak solutions in cfd, International journal for numerical methods in fluids 57 (9) (2008) 1153–1170.

[19] J. Duchon, R. Robert, Inertial energy dissipation for weak solutions of incompressible euler and navier-stokes equations, Nonlinearity 13 (1) (2000) 249.

[20] L. Onsager, Statistical hydrodynamics, Il Nuovo Cimento (1943-1954) 6 (1949) 279–287.

[21] G. L. Eyink, K. R. Sreenivasan, Onsager and the theory of hydrodynamic turbulence, Reviews of modern physics 78 (1) (2006) 87.

[22] J. Hoffman, C. Johnson, Computational Turbulent Incompressible Flow: Applied Mathematics: Body and Soul 4, Vol. 4, Springer, 2007.

[23] J. Hoffman, J. Jansson, R. Vilela De Abreu, Adaptive modeling of turbulent flow with residual based turbulent kinetic energy dissipation, Computer Methods in Applied Mechanics and Engineering 200 (37) (2011) 2758–2767.

[24] K. Eriksson, D. Estep, P. Hansbo, C. Johnson, Introduction to adaptive methods for differential equations, Acta numerica 4 (1) (1995) 105–158.

[25] R. Becker, R. Rannacher, An optimal control approach to a posteriori error estimation in finite element methods, Acta Numerica 2001 10 (2001) 1–102.

[26] J. Hoffman, C. Johnson, Blow up of incompressible euler solutions, BIT Numerical Mathematics 48 (2) (2008) 285–307.

[27] R. V. Abreu, N. Jansson, J. Hoffman, Adaptive computation of aeroacoustic sources for a rudimentary landing gear, International Journal for Numerical Methods in Fluids 74 (6) (2014) 406–421.

[28] R. V. de Abreu, N. Jansson, J. Hoffman, Adaptive computation of aeroacoustic sources for a rudimentary landing gear using lighthills analogy, AIAA Paper 2942 (2011) 2011.

[29] P. R. Spalart, Detached-eddy simulation, Annual Review of Fluid Mechanics 41 (2009) 181–202.

[30] J. Hoffman, N. Jansson, A computational study of turbulent flow separation for a circular cylinder using skin friction boundary conditions, in: Quality and Reliability of Large-Eddy Simulations II, Springer, 2011, pp. 57–68.

[31] R. V. de Abreu, N. Jansson, J. Hoffman, Computation of aeroacoustic sources for a complex nose landing gear geometry using adaptivity, in: Proceedings of the Second Workshop on Benchmark problems for Airframe Noise Computations (BANC-II), Colorado Springs, 2012.

[32] J. Hoffman, J. Jansson, N. Jansson, R. V. de Abreu, Time-resolved adaptive fem simulation of the dlr-f11 aircraft model at high reynolds number.

[33] P. Moin, J. Kim, Tackling turbulence with supercomputers, Scientific American 276 (1) (1997) 46–52.

[34] L. Prandtl, On fluid motions with very small friction, in: Verhldg. 3 Int. Math. Kongress, Wiley, 1904, pp. 484–91.

[35] J. Hoffman, Simulation of turbulent flow past bluff bodies on coarse meshes using general galerkin methods: drag crisis and turbulent euler solutions, Computational Mechanics 38 (4-5) (2006) 390–402.

[36] J. Hoffman, C. Johnson, Resolution of dalemberts paradox, Journal of mathematical fluid mechanics 12 (3) (2010) 321–334.

[37] M. Ainsworth, J. T. Oden, A posteriori error estimation in finite element analysis, Computer Methods in Applied Mechanics and Engineering 142 (1) (1997) 1–88.

[38] J. Hoffman, C. Johnson, Adaptive finite element methods for incompressible fluid flow, in: Error estimation and adaptive discretization methods in computational fluid dynamics, Springer, 2003, pp. 97–157.

[39] J. Hoffman, Computation of mean drag for bluff body problems using adaptive dns/les, SIAM Journal on Scientific Computing 27 (1) (2005) 184–207.

[40] W. Bangerth, R. Rannacher, Adaptive finite element methods for differential equations, Springer, 2003.

[41] J. Hoffman, J. Jansson, R. Vilela de Abreu, N. C. Degirmenci, N. Jansson, K. Müller, M. Nazarov, J. H. Spühler, Unicorn: Parallel adaptive finite element simulation of turbulent flow and fluid–structure interaction for deforming domains and complex geometry, Computers & Fluids 80 (2013) 310–319.

[42] The fenics project.

[43] N. Jansson, J. Hoffman, J. Jansson, Framework for massively parallel adaptive finite element computational fluid dynamics on tetrahedral meshes, SIAM Journal on Scientific Computing 34 (1) (2012) C24–C41.

[44] N. Jansson, J. Hoffman, M. Nazarov, Adaptive simulation of turbulent flow past a full car model, in: High Performance Computing, Networking, Storage and Analysis (SC), 2011 International Conference for, IEEE, 2011, pp. 1–8.

[45] Parmetis - parallel graph partitioning and fill-reducing matrix ordering.

[46] Petsc - portable, extensible toolkit for scientific computation.

[47] J. Hoffman, Adaptive simulation of the subcritical flow past a sphere, Journal of Fluid Mechanics 568 (2006) 77–88.

[48] J. Hoffman, Efficient computation of mean drag for the subcritical flow past a circular cylinder using general galerkin g2, International journal for numerical methods in fluids 59 (11) (2009) 1241–1258.

[49] M. Zdravkovich, Flow around circular cylinders, vol. 1. fundamentals, Journal of Fluid Mechanics 350 (1997) 377–378.

[50] A. Korotkin, The three-dimensional character of a cross flow around a circular cylinder, TsAGI, Uchenye Zapiski 4 (5) (1973) 26–33.

[51] J. S. Humphreys, On a circular cylinder in a steady wind at transition reynolds numbers, Journal of Fluid Mechanics 9 (04) (1960) 603–612.

[52] B. Gölling, Experimentelle untersuchungen des laminar-turbulenten überganges der zylindergrenzschichtströmung, Ph.D. thesis, DLR (2001).

[53] G. Schewe, Reynolds-number effects in flow around more-or-less bluff bodies, Journal of Wind Engineering and Industrial Aerodynamics 89 (14) (2001) 1267–1289.

[54] J. Jansson, J. Hoffman, N. Jansson, Simulation of 3d unsteady incompressible flow past a naca 0012 wing section, CTL Technical Report kth-ctl-4023.

[55] J. Hoffman, J. Jansson, R. V. de Abreu, Computation of slat noise sources using adaptive fem and lighthills analogy, in: 19th AIAA/CEAS Aeroacoustics Conference, 2013.

[56] M. Nazarov, J. Hoffman, On the stability of the dual problem for high reynolds number flow past a circular cylinder in two dimensions, SIAM Journal on Scientific Computing 34 (4) (2012) A1905–A1924.

[57] Q. Wang, J.-H. Gao, The drag-adjoint field of a circular cylinder wake at reynolds numbers 20, 100 and 500, Journal of Fluid Mechanics 730 (2013) 145–161.